Supramolecular Assemblies of Quaternary Ammonium Cations and Halide Anions in the Gas Phase: ESMS-FTICR Data and Computer Modelling

Catrin Hasselgren,[a] Keith Fisher,[b] Susan Jagner,[a] and Ian Dance[b]*

Abstract: Supramolecular aggregates of tetraalkylammonium halides (R_4NX) are formed by electrospray out of acetonitrile solution. Mass spectrometry reveals 88 charged aggregates for R = Me, Et, Bu; X = Br, I, ranging up to $[(Bu_4N)_{39}Br_{42}]^{3-}$ in size. With the objective of improving calculations of intermolecular energies for supramolecular aggregates of ions, calibrated semi-empirical potentials for inter-ion interactions have been developed and applied to these aggregates. The accuracy of the calculated energies is supported by the measured collisional dissociation energy of $(Et_4N^+)_4\ (I^-)_5$. Energy optimisations indicate that the probable structures have the halide ions dispersed in a matrix of cations, which, for Bu_4N^+, can be mutually attractive. The aggregates are structurally fluid, with multiple structures separated by $4-8\ kJ\,mol^{-1}$. The energy calculations are entirely consistent with the observed formation of large aggregates, and of multiply charged anions. It is estimated that the cohesive energies of supramolecular assemblies of ions such as these reach about $40\ kJ\,mol^{-1}$ per constituent ion.

Keywords: anions · cations · electrostatic interactions · gas-phase chemistry · mass spectrometry · supramolecular chemistry

Introduction

We are investigating the supramolecularity of compounds that contain polyatomic cations and anions. A principal source of information is the crystal packing of these compounds, and we have investigated,[1–7] analysed and classified[2–7] the interion packing in a large number of ammonium and phosphonium salts with diverse anions. Analyses of the data in the Cambridge Structural Database allow detailed descriptions of the geometries of recognisable crystal supramolecular motifs, but do not provide the energy data which are the fundamental causative influences. However, the repeated occurrence of motifs in numerous and diverse crystals is clear qualitative evidence that the motifs are competitively attractive. The intermolecular energies can be calculated, using density functional theory for relatively small systems,[8] and by semi-empirical potentials, but these require careful calibration of the atom···atom potentials used for the van der Waals and electrostatic energies. The thermochemical data required for these calibrations are rarely available for the polyatomic compounds of interest, and for which crystal structures are available. We have not found in the literature data on the intermolecular energies for polyatomic cations and anions.

Dissociation energies can in principle be measured for supramolecular aggregates in the gas phase.[9, 10] Therefore we are investigating the generation and properties of gaseous aggregates analogous to those investigated in the crystal phase. In particular, electrospray ionisation of solutions of the relevant cation·anion combinations can generate aggregates of cations + anions as part of the process of reduction of net charge density during electrospray desolvation.[11–14] Electrospray mass spectrometry (ESMS) is valuable because large aggregates containing many cations and anions can be observed—particularly when the aggregate has multiple net charge—and these larger aggregates simulate more closely the extended crystal phase. A further advantage is that the complication of solvation is normally absent from the gas phase and the crystal phase, simplifying investigations of fundamental supramolecular aggregates.

The combination of ES for generation of aggregates of polyatomic ions, and Fourier transform ion cyclotron resonance (FTICR) for investigation of their dissociation and reactivity, is valuable. Herein we report ES-FTICR investigations of some combinations of tetralkylammonium cations and halide anions, together with calculations of their structures and energies. The generation of some quaternary ammonium and phosphonium (Me_4N^+, Pr_4N^+, $MeEt_3N^+$, Et_4P^+) bromides and (Me_4N^+, Et_4P^+) chlorides, all as mononegative ions, has been described previously.[15] Hop,[16] seeking mass calibrants, reported the generation of large

[a] C. Hasselgren, Prof. S. Jagner
Department of Inorganic Chemistry
Chalmers University of Technology
SE-412 96, Göteborg (Sweden)

[b] Prof. I. Dance, K. Fisher
School of Chemistry, University of New South Wales
Sydney NSW 2052 (Australia)
E-mail: I.Dance@unsw.edu.au

  0947-6539/00/0620-3671 $ 17.50+.50/0

negative and positive aggregates by electrospray of $Et_4N^+ I^-$ in acetonitrile. The influence of solvents on ion pairing involving dications has been investigated.[17]

Our first question was what aggregates of tetraalkylammonium cations and halide anions can be generated and studied in the gas phase? We observe large aggregates, containing up to 80 individual ions, which raise further questions. What are their structures? What are their cohesive energies, and can their dissociation energies be measured in the gas phase? Since the tetraalkylammonium cations are larger than the monatomic anions in these aggregates, the cations must be in contact. This relates to another fundamental question about the supramolecular energies of condensed phases containing ions. The inter-ion energies comprise van der Waals attractions and coulombic energies which are both attractive and repulsive. As the number of atoms in the ion increases the van der Waals attractions increase, and the ion charges are dispersed over more atoms, the balance of energy contributions being changed to a point where *ions of the same charge are attractive*. Therefore, in order to address these questions, we have used semi-empirical intermolecular potentials to calculate the energies of our new aggregates, and to explore structure by energy minimisation.

Mass Spectrometric Methods

The salts Me_4NBr, Et_4PCl, Et_4NBr, Et_4NI, Bu_4NBr, Me_3PhNI, and Me_3BzNCl were reagent grade. The acetonitrile solvent was HPLC grade. Solution concentrations were approximately 1 mg per 10 mL.

Experiments were carried out on a Bruker BioAPEC II FTICRMS equipped with a 7T super conducting magnet, with an external electrospray (Analytica) ion source. This instrument was pumped by three cryogenic pumps and a turbo molecular pump. The four stage differential pumping allowed the transfer of ions from the one atmosphere ion source through a capillary to the cell region maintained at a pressure of 1×10^{-8} Pa. A syringe pump was used to spray samples at 60 $\mu L\,h^{-1}$ through a spray needle with a 0.1 mm tip. The spray needle was grounded and approximately 1 cm from a nickel coated end of a quartz capillary tube. Nitrogen heated to 280 °C was used as drying gas.

For negative ions the capillary voltage was maintained at 4 kV and the outlet of the capillary into the pumped source was varied between -10 and -400 V. Typically the capillary voltage was -50 V with the skimmer voltage of -5 V. The outlet of the capillary entered a region with a pressure of 4×10^{-4} Pa. Emerging from the capillary the ions were accelerated towards a skimmer maintained at -5 V (or $+5$ V for positive ions). Ions passing through the skimmer were trapped in a hexapole ion trap for a controlled period (1 or 2 s) to accumulate ions. The stored ions were released as a package and guided to the ICR cell using a series of ion lenses.

The ion $(Et_4N)_4I_5^-$ was isolated in the cell, and on-resonance collision-induced dissociation (ORCID) carried out. The selected ions were accelerated in the presence of argon at 1×10^{-6} Pa by irradiation (rf pulse) at the cyclotron resonance frequency of the ion. The ion acceleration energy pulse length and collision time were varied to obtain the minimum energy to effect dissociation in one collision.

The centre of mass translational kinetic energy E_{com} of an activated ion was calculated using Equation (1), where m_t is the mass of the argon target, m_p

$$E_{com} = [m_t/(m_t + m_p)](0.81\,V_{pp}/d)^2 q(t_{rf})^2/8m_p \quad (1)$$

is the mass of the selected ion, 0.81 is the geometry factor of the cylindrical cell, V_{pp} is the peak to peak voltage of the rf pulse, d is the diameter of the cell (6 cm), q is the electronic charge and t_{rf} is the length of the excitation pulse.[18, 19]

Computational Methods

Our model for intermolecular energies is based on summed interatomic energies.[20] The van der Waals potential between two non-bonded atoms separated by d_{ij} is expressed by Equation (2), in which d^a_{ij} is the distance between atoms i and j at which the interaction energy is most negative, with the magnitude e^a_{ij}.[21] The two important parameters are d^a_{ij} and e^a_{ij}, obtained by combination of atom parameters [Equations (3) and (4)]. The atom radii r^a are larger than the conventional crystallographic van der Waals radii, which correspond to slightly repulsive energies.[21]

$$E^{vdW}_{ij} = e^a_{ij}\,[(d_{ij}/d^a_{ij})^{-12} - 2(d_{ij}/d^a_{ij})^{-6}] \quad (2)$$

$$d^a_{ij} = r^a_i + r^a_j \quad (3)$$

$$e^a_{ij} = (e^a_i e^a_j)^{0.5} \quad (4)$$

The interatomic electrostatic energy is expressed as Equation (5), in which q are the atom partial charges and ε is the permittivity of the medium.

$$E^{elec}_{ij} = q_i q_j/\varepsilon d_{ij} \quad (5)$$

The total intermolecular energy is given by Equation (6).

$$E^t = \Sigma_{ij}(E^{vdW}_{ij} + E^{elec}_{ij}) \quad (6)$$

The parameters required are the e^a, r^a, q for each atom, and ε. Our parametrisation of e^a and r^a uses three sources of information: 1) the parameters in the literature; 2) an overview of these parameters for all atom types in this region of the periodic table, and modulation according to charge type (e^a and r^a are correlated and increase with the negative charge state of the atom);[22] and 3) testing against the crystal packing geometry for $R_4N^+ X^-$ compounds. As guides and tests for our models we examined the crystal structures of $Bu_4N^+Br^-$ [RABTIX] (Cambridge Structural Database refcodes in square brackets) $Bu_4N^+I^-$ [RABTET], $Bu_4N^+Br_3^-$ [JEPGUG], $Et_4N^+Br^-$ [TUDQEO], $Bu_4N^+I_3^-$ [NBAMTI10], $Et_4N^+I^-$, and $Me_4N^+I^-$, from which it is concluded that H···Br intermolecular distances are in the range 3.0–3.3 Å, and H···I intermolecular distances are in the range 3.2–3.6 Å. Our parameters (see below) give H···Br distances in the range 3.2–3.4 Å.

Full negative charges are used for the halide anions. Our parametrisation of the atom partial charges for the cations is informed by both quantum calculations (Mulliken, Hirshfeld and electrostatic potential calculations) and the charge equilibration (QEq) method of Rappe and Goddard.[23] The values of q are N, -0.28; H, 0.14; C_{methyl}, -0.10; C_{1ethyl}, -0.11; C_{2ethyl}, -0.27; C_{1butyl}, -0.12; C_{2butyl}, -0.24; C_{3butyl}, -0.26; C_{4butyl}, -0.32.

An important and influential parameter is the permittivity ε for the electrostatic energies [Eq. (5)]. What is the permittivity (or dielectric constant) inside an aggregate of R_4N^+ ions and X^- ions, without solvent? In approaching this we note the contributions to ε from the electronic polarisabilities and from possible reorientation of the component polar components,[24] and other complexities for modelling within polar macromolecules.[25] Thus the dielectric constant of water at low frequency is 80 (20 °C), but only about four when measured at high frequencies not permitting reorientation.[24] In view of the electronic polarisabilities of the halide ions in the aggregates, their charged nature, their intramolecular fluidity in the gas phase, and the fundamental limitations of the use of a monopole model for electrostatic energies, [26] we adopt the approximation of Equation (7).

$$\varepsilon = 2\,d_{ij} \quad (7)$$

The derived parameters for the relevant atom types are C(alkyl), $r^a = 2.04$ Å, $\varepsilon = 0.154$ kJ mol^{-1}; H, $r^a = 1.62$ Å, $\varepsilon = 0.084$ kJ mol^{-1}; N(quaternary), $r^a = 1.9$ Å, $\varepsilon = 0.46$ kJ mol^{-1}; Br^-, $r^a = 2.3$ Å, $\varepsilon = 2.2$ kJ mol^{-1}; I^-, $r^a = 2.4$ Å, $\varepsilon = 2.8$ kJ mol^{-1}.

Calculations used the Discover program.[27] The CVFF force field was used for the intramolecular energies of the cations.

0947-6539/00/0620-3672 $ 17.50+.50/0 *Chem. Eur. J.* **2000**, *6*, No. 20

Results

Negative ion spectra were obtained for Me_4NBr, Et_4PCl, Et_4NBr, Et_4NI, Bu_4NBr, Me_3PhNI and Me_3BzNCl in acetonitrile, and positive ion spectra for Bu_4NBr in acetonitrile. Methanol gave poor spectra. A negative ion spectrum for Bu_4NBr in the high mass range is shown in Figure 1, illustrating the formation of mono-, di- and tri-negative aggregates.

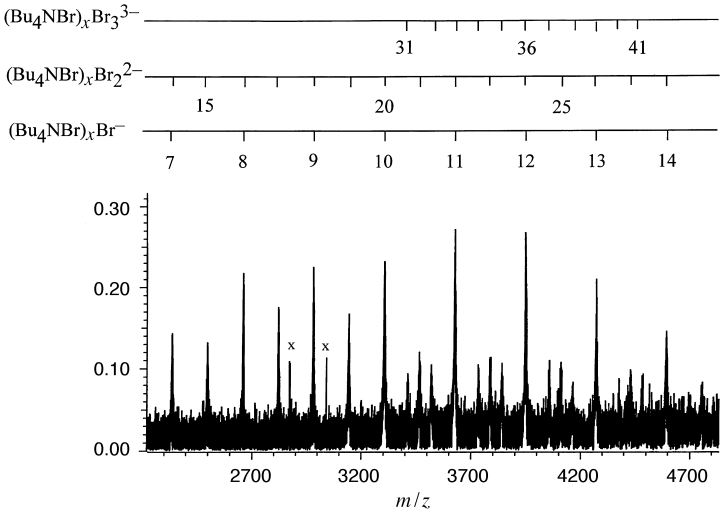

Figure 1. Negative ion ESI mass spectrum for a solution of Bu_4NBr in acetonitrile. Peak intensity is plotted relative to $[Bu_4NBr_2]^- = 1$. Peaks x are instrument artefacts.

The full range of observed aggregates is graphed in Figure 2.

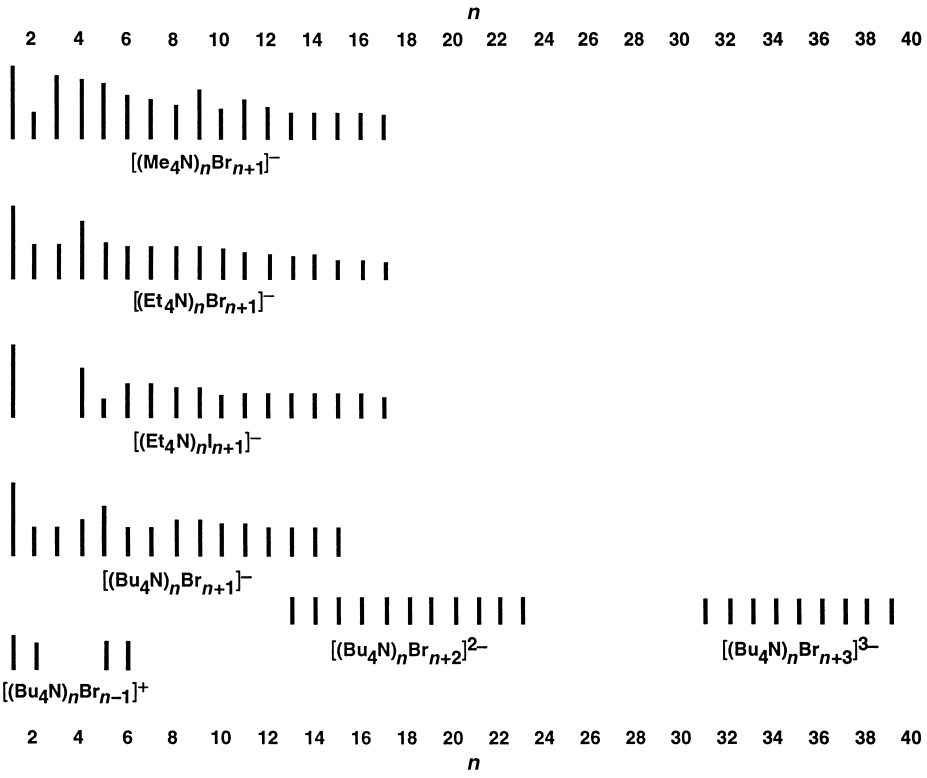

Figure 2. Chart of observed ions. Line lengths indicate relative intensities.

Collision-induced dissociation: Isolation of $[(Et_4N)_4I_5]^-$ in the ICR cell and collision-induced dissociation (CID) with Ar yielded $[(Et_4N)I_2]^-$ as the only product. The CID experiment was operated in the on-resonance mode, with a constant pressure of Ar, and gave an energy of dissociation of 100 kJ mol^{-1}. This result is discussed further below in conjunction with the relevant calculated energies.

Isolation of $[(Et_4N)_4Br_5]^-$ resulted in its dissociation, in the absence of acceleration. We were unable to effect meaningful CID experiments with other negative ions, but obtained two results with related positive ions: $[(Me_3PhN)_4I_3]^+ \rightarrow [(Me_3PhN)_2I]^+$ $\Delta E = 600$ kJ mol^{-1}, and $[(Me_3BzN)_5Cl_4]^+ \rightarrow [(Me_3BzN)_2Cl]^+$ $\Delta E = 320$ kJ mol^{-1}.

There are considerable experimental uncertainties in these results, due to difficulty in determining the threshold for dissociation.

Computer models of observed aggregates: We have postulated structures, and optimised them by minimisation of the total of all intermolecular energies and the intramolecular energy for the conformationally variable cations. For each aggregate composition a number of starting geometries were investigated, and in some cases optimised structures were distorted and re-optimised, as a crude procedure to search for alternative minima. It soon became evident that the energy surface, at least for the larger aggregates, was relatively flat. Molecular dynamics were not calculated. The structures presented here had the lowest total energy for each composition. The examples presented are for the larger cation Bu_4N^+ with smaller anion Br^-, and smaller cation Et_4N^+ with larger anion I^-.

We present first results for the geometries of some smaller aggregates, in order to demonstrate some of the fundamental principles. Figure 3 shows the optimised structures of combinations of a single cation and single anion, specifically of $Et_4N^+I^-$ and $Bu_4N^+Br^-$. The anion is not located on the $\bar{4}$ axis of the cation due to the small repulsive contribution involving the partial negative charge on N. Two Bu_4N^+ ions form a cohesive pair, with various conformations of intertwined arms (Figure 4). This is because the net van der Waals attraction exceeds the net electrostratic repulsion. Two Et_4N^+ cations are not cohesive. In the association of two anions with one cation (Figure 5) the anions need not be directly opposed, but their positions are determined by the attractive interactions with alkyl chains.

Figures 6 and 7 show structures with two and three cations respectively associated with three anions. It is evident that

Figure 3. Optimised structures for single cations with single anions: the anion is associated with one alkyl group rather than located on the pseudo $\bar{4}$ axis of the cation.

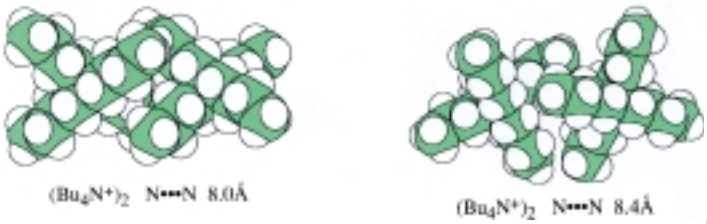

Figure 4. Two energy minima for an attractive pair of Bu_4N^+ cations.

Figure 5. Optimised structures for associations of two anions with one cation.

three Bu_4N^+ ions can form an intimate aggregate with three Br^-, partially enveloping the anions with substantial areas of cation $\cdots$ anion and cation $\cdots$ cation contact. However, three small Et_4N^+ ions leave three I^- ions largely exposed. Figure 8 shows two structures for the composition $(R_4N^+)_4(X^-)_5$, on which the CID experiment was effected. Note that the aggregates are approximately discoid, with insufficient atoms to be globular.

We have not optimised all of the compositions seen in the ESMS. Instead we have considered representative larger sizes, again seeking structural principles. One question which arises for larger aggregates is whether there is a segregation of cations on the inside and anions on the outside, or of the reverse, or whether there is an alternation of oppositely charged ions, in a "fruit-cake" structure. In the larger aggregates the locations

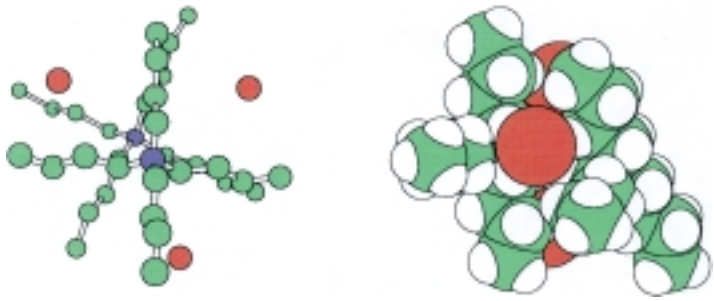

Figure 6. Skeletal (H atoms omitted) and space-filling different views of $(Bu_4N^+)_2(Br^-)_3$, showing (left) how the arms of the cations are approximately eclipsed by their mutual attractions, and (right) how the three anions are approximately symmetrically arrayed between the two cations.

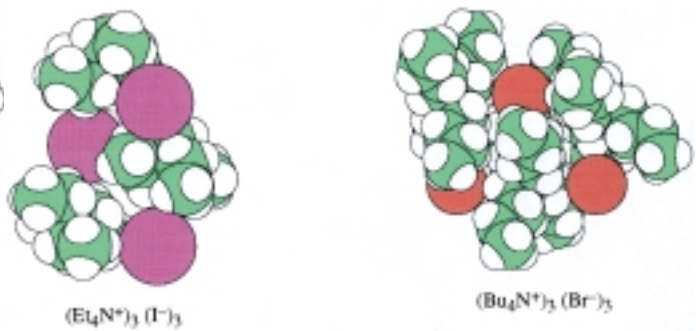

Figure 7. Two structures for $(R_4N^+)_3(X^-)_3$ which have a symmetrical and approximately coplanar array of cations and anions.

of ions can be obscured by the numerous atoms, and so we use two types of pictorial representation: the space-filling picture for all atoms shows the nature of the surface, while the second representation (same view direction) shows just the N and anion atoms, with colour shading according to distance from the viewer.

Starting structures for the larger aggregates were generated as relatively symmetrical arrays of ions. As an illustration, the initial array of cation centres and anions for $(Bu_4N^+)_8$ $(Br^-)_9$ had threefold symmetry, as shown in Figure 9 (c). The alkyl chains could not follow this symmetry, and optimisation yielded quite unsymmetrical structures (Figure 9).

The composition $(cation)_{12}(anion)_{13}$, observed for all systems, has been modelled with several different starting

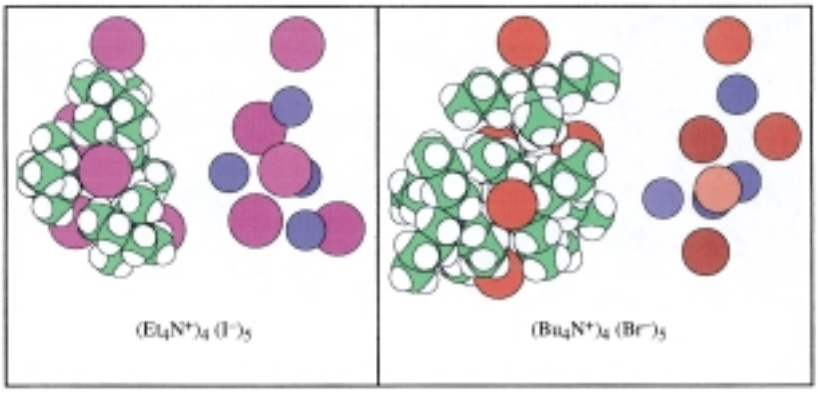

Figure 8. Two structures of $(R_4N^+)_4(X^-)_5$. Each structure is drawn in full on the left, and on the right with the only the N and halide skeleton, using colour darkening away from the viewer. Note that the array of cation and anion sites is approximately planar, and that these aggregates are not yet large enough to be fully globular.

0947-6539/00/0620-3674 $ 17.50+.50/0 *Chem. Eur. J.* **2000**, *6*, No. 20

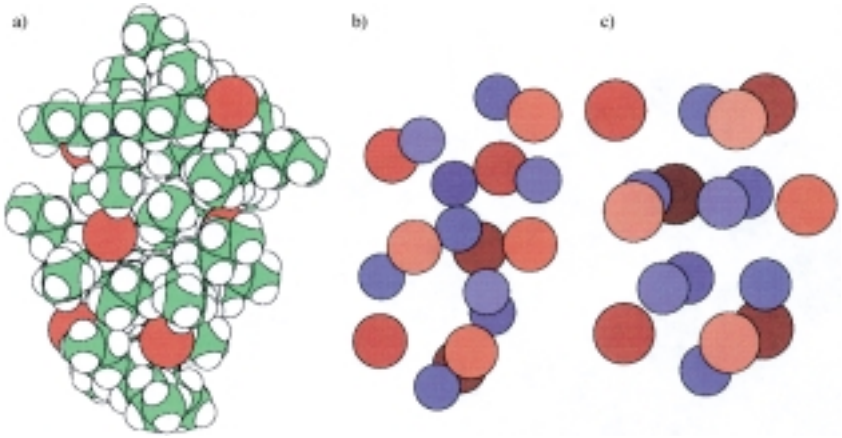

Figure 9. a) and b) The optimised structure of $(Bu_4N^+)_8(Br^-)_9$, starting from the array c) of ion centres which has threefold symmetry about the vertical axis.

structures, based on the regular polyhedra (cuboctahedron, icosahedron) with twelve vertices, empty, or centred for 13 points, and the threefold structures based on stacks of A_3B_3 hexagons.[28] We present the result of one such optimisation in Figure 10. The composition $(cation)_{13}(anion)_{14}$ is that of the

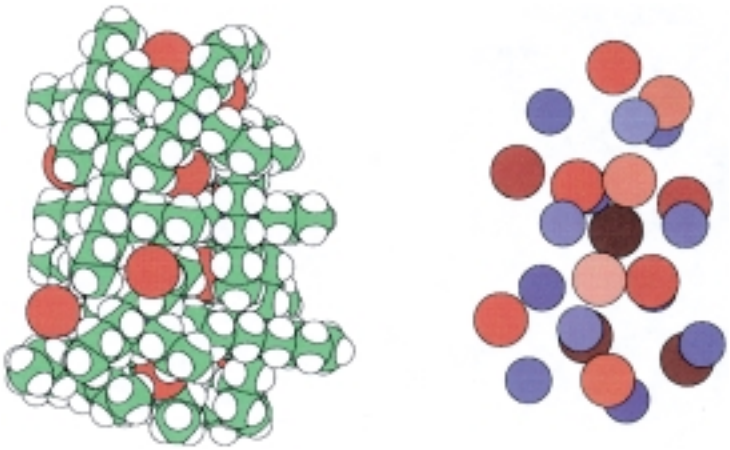

Figure 10. An optimised structure of $(Bu_4N^+)_{12}(Br^-)_{13}$.

unit cell of the face-centred cubic array, common in alkali metal halides, but as shown in Figure 11 this order and symmetry are lost in the optimised structure of $(Bu_4N^+)_{13}(Br^-)_{14}$.

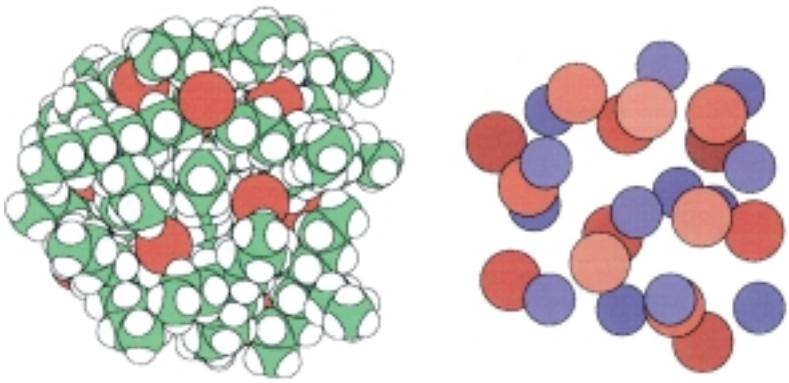

Figure 11. The optimised structure of $(Bu_4N^+)_{13}(Br^-)_{14}$, which started from a face-centred cubic array of cations and anions.

We have also investigated $(Bu_4N^+)_{24}(Br^-)_{25}$, with several starting structures inspired by and derived from the structures of binary metal carbides (metallocarbohedrenes) of composition $Cu_{25}C_{24}$,[29] appropriately expanded. However no new insight evolved from this composition, and so we move to the largest aggregate investigated, namely $(Bu_4N^+)_{40}(Br^-)_{41}$. We used various starting structures which concentrated 20 cations in the core, or which concentrated 20 anions in the core, but in both cases the optimised structures showed no segregation of either ion, and a "fruit cake" structure resulted. Figure 12 shows how a concentration of cations in the centre of $(Bu_4N^+)_{40}(Br^-)_{41}$ optimises to a more regular distribution of cations.

The preceding models contained one excess anion, for the series $(Bu_4N^+)_n(Br^-)_{n+1}$, whereas the higher mass aggregates observed possess two or three excess anions. Models for these are readily developed in the same way. In order to demonstrate the calculated stability of aggregates with excess anions or with excess cations, we show the optimised structures for some extremes. The aggregation of six cations and one anion, namely $[(Bu_4N^+)_6(Br^-)]^{5+}$, is stable (Figure 13), as is the aggregation of one cation and four anions, in $[(Bu_4N^+)(Br^-)_4]^{3-}$ (Figure 14). It is significant that the coulombic repulsions between four Br^- are overcome by association with one Bu_4N^+. A structure with one Bu_4N^+ ion and eight Br^- anions dissocated four Br^- to become the structure in Figure 14.

It was obvious during the modelling that there are multiple structures for aggregates with more than one or two cations. These multiple minima on the energy surfaces had similar energies, and apparently small energy barriers between them. Examination of structure during the energy minimisation processes showed frequent relative movements of ions relative to each other, and the initial and optimised structures presented in Figure 12 demonstrate further the mobility of these aggregates. The concept of a liquid drop should be imposed on the static pictures presented, and it is clear that there is no preferred order for aggregates of Bu_4N^+ cations with monatomic anions. The cations tend to have elongated conformations for their butyl arms, and the main barrier to geometry change in the aggregates is in the rearrangements of entangled arms. While there are no strong repulsions between Et_4N^+ ions or between Bu_4N^+ ions, the structures generally have desegregated ions,

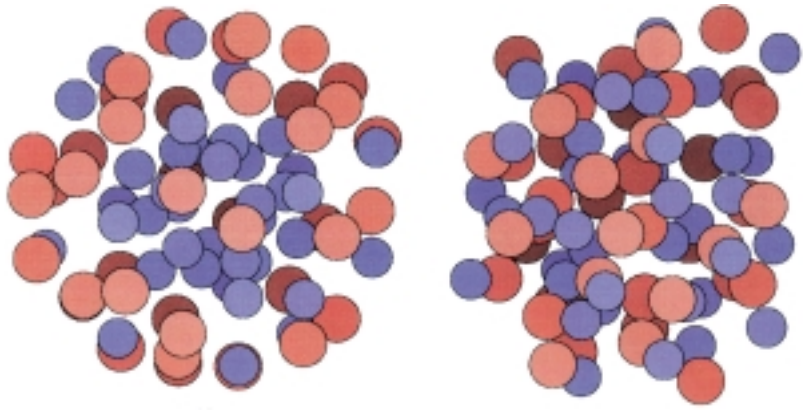

Figure 12. This figure shows the starting (left) and optimised (right) structures for $(Bu_4N^+)_{40}(Br^-)_{41}$. The starting structure contained a core of 20 cations.

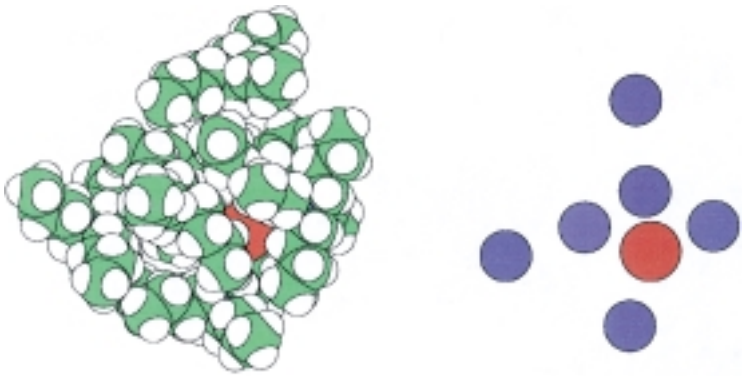

Figure 13. The optimised structure of $[(Bu_4N^+)_6(Br^-)]^{5+}$.

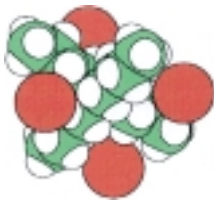

Figure 14. The optimised structure of $[(Bu_4N^+)(Br^-)_4]^{3-}$.

and the "fruit cake" structural concept of smaller anions dispersed in a matrix of larger cations is appropriate.

Energies: The energy minimised is the sum of the intermolecular and intramolecular energies, but the latter are (by definition) not on an absolute scale, and so the total energies minimised do not directly reveal the cohesive energies of the aggregates. Therefore we have evaluated the components of the intermolecular energies for some of the optimised structures presented in the figures. These are presented in Table 1, as values for cation$\cdots$cation energies, cation$\cdots$anion energies and anion$\cdots$anion energies, and the total intermolecular energy E^t. In Table 2 there are values of the intermolecular energies for additional aggregates, and, in order to compare aggregates of different sizes, the intermolecular energies per ion (E^t_{ion}) are listed.

Several patterns are evident in these total energies, which include the van der Waals and electrostatic components.

1) The cation$\cdots$cation energies in these aggregates are weakly attractive or repulsive, in the range -5 to $+10$ kJ mol^{-1}, and are more attractive for larger R_4N^+ ions. This is consistent with the calculated result that $(Bu_4N^+)_2$ is cohesive, but $(Et_4N^+)_2$ is not.
2) Anion$\cdots$anion repulsions in these aggregates are in the range $+2$ to $+17$ kJ mol^{-1}.
3) Anion$\cdots$cation energies, always attractive, range up to about 35 kJ mol^{-1}, depending on the juxtapositions of the ions.
4) The net intermolecular energy *per constituent ion* (E^t_{ion}, Table 2) is about -20 kJ mol^{-1} for $R_4N^+(X^-)_2$, about -30 kJ mol^{-1} for $(R_4N^+)_2(X^-)_3$ and about -33 kJ mol^{-1} for $(R_4N^+)_4(X^-)_5$, and not very dependent on the identity of R or X. This energy E^t_{ion} is an indicator of the relative cohesion of these aggregates of different sizes and with different components. Extrapolation of the results in Table 2 to larger aggregates suggests that the cohesive energies per constituent ion could reach -40 kJ mol^{-1}.
5) The intermolecular energy per constituent ion is hardly affected by the net charge of the aggregate, and is but marginally better for $(Et_4N^+)_2I^-$ relative to $Et_4N^+(I^-)_2$, or for $(Bu_4N^+)_2Br^-$ relative to $Bu_4N^+(Br^-)_2$.
6) The variability of the values in Tables 1 and 2 reflects differences in structure. Differences in local structure are also clearly evident (see Figures 7–12) for aggregates with more than about five ions. The magnitude of the variability of inter-ion energies is about 4–8 kJ mol^{-1}, and we expect that this would also be the magnitude of the energy barriers to be expected between alternative structures.

An objective of this research was to obtain experimental data relating to intermolecular energies in aggregates of tetraalkylammonium halides. One datum was obtained, namely that about 100 kJ mol^{-1} was required to collisionally dissociate $[(Et_4N^+)_4(I^-)_5]^-$ to $[Et_4N^+(I^-)_2]^-$ plus unobserved products. There are four possible sets of products, and for each of these the calculated energy for dissociation (using the results in Table 2) is listed in Table 3. The pathway which generates the unobservable neutral aggregates $[(Et_4N^+)_2(I^-)_2]^0$ and $[Et_4N^+I^-]^0$ in addition to the observed $[Et_4N^+(I^-)_2]^-$ has a calculated energy which agrees with the measured collisional dissociation energy: we note that these are calculations of internal energy. The pathway which yields an intact $[(Et_4N^+)_3(I^-)_3]^0$ neutral aggregate is indicated to be least likely. However we emphasise that there are considerable uncertainties about the collisionally induced dissociative process and in our experimental measurement of the threshold dissociation energy. These uncertainties are reflected in the failure of similar experiments with other ions.

0947-6539/00/0620-3676 $ 17.50+.50/0 *Chem. Eur. J.* **2000**, *6*, No. 20

Table 1. Calculated intermolecular energies for aggregated ions.

Aggregate	Figure	Intermolecular energy [kJ mol^{-1}]			
		cation $\cdots$ cation	cation $\cdots$ anion	anion $\cdots$ anion	total, E^t
$Et_4N^+I^-$	3 (left)	–	−34.6	–	−34.6
$Bu_4N^+Br^-$	3 (right)	–	−34.2	–	−34.2
$(Bu_4N^+)_2$	4	−2.0	–	–	−2.0
$Et_4N^+(I^-)_2$	5 (left)	–	−34.4, −31.6	+8.2	−57.8
$Bu_4N^+(Br^-)_2$	5 (right)	–	−31.7, −34.0	+7.7	−58.0
$(Et_4N^+)_3(I^-)_3$	7 (left)	+7.4	−33.8, −34.0	+14.1	−188
		+9.4	−5.5, −34.5	+11.2	
		+9.8	−8.3, −31.5	+8.5	
			−31.4, −34.5		
			−34.5		
$(Bu_4N^+)_3(Br^-)_3$	7 (right)	+4.9	−33.1, −31.8	+7.6	−209
		−1.8	−5.6, −32.0	+11.3	
		−2.4	−6.1, −33.2	+11.9	
			−31.7, −33.6		
			−33.3		
$(Et_4N^+)_4(I^-)_5$	8 (left)	+6.3	−31.6, −31.4	+5.8	−300
		+9.5	−4.9, −33.4	+2.5	
		+10.2	−6.0, −2.8	+9.1	
		+9.5	−30.5, −34.1	+2.7	
		+9.1	−7.2, −31.0	+8.9	
		+9.8	−5.0, −28.5	+17.2	
			−31.4, −31.1	+14.6	
			−30.7, −4.7	+5.8	
			−33.3, −5.7	+13.1	
			−31.0, −30.6	+10.8	
$(Bu_4N^+)_4(Br^-)_5$	8 (right)	+2.3	−33.8, −31.8	+7.6	−300
		−5.1	−7.4, −16.6	+7.4	
		+3.2	−3.7, −15.9	+5.1	
		+0.5	−8.8, −30.7	+2.1	
		+4.3	−4.4, −3.1	+8.7	
		+1.1	−18.7, −25.0	+16.0	
			−32.9, −32.6	+8.3	
			−5.1, −3.6	+7.9	
			−32.6, −7.9	+3.8	
			−32.8, −33.6	+8.0	

Table 2. Intermolecular energies [kJ mol^{-1}] for aggregates of Me_4N^+, Et_4N^+, Bu_4N^+ with Br^- and I^-, as total E^t, and as energy per ion, E^t_{ion}.

Aggregate	E^t	E^t_{ion}
$Me_4N^+(Br^-)_2$	−67.0	−22.3
$(Me_4N^+)_2(Br^-)_3$	−154	−30.8
$(Me_4N^+)_3(Br^-)_4$	−241	−34.5
$(Me_4N^+)_4(Br^-)_5$	−317	−35.3
$Et_4N^+(Br^-)_2$	−60.6	−20.2
$(Et_4N^+)_2(Br^-)_3$	−149	−29.8
$(Et_4N^+)_3(Br^-)_4$	−228	−32.6
$(Et_4N^+)_4(Br^-)_5$	−286	−31.8
$Et_4N^+I^-$	−34.6	−17.3
$Et_4N^+(I^-)_2$	−57.8	−19.3
$(Et_4N^+)_2I^-$	−59.9	−20.0
$(Et_4N^+)_2(I^-)_2$	−108	−27.0
$(Et_4N^+)_3(I^-)_3$	−188	−31.3
$(Et_4N^+)_4(I^-)_5$	−300	−33.3
$Bu_4N^+Br^-$	−34.2	−17.1
$Bu_4N^+(Br^-)_2$	−58.0	−19.3
$(Bu_4N^+)_2Br^-$	−65.4	−21.8
$(Bu_4N^+)_2(Br^-)_2$	−122	−30.4
$(Bu_4N^+)_2(Br^-)_3$	−153	−30.6
$(Bu_4N^+)_3(Br^-)_3$	−209	−34.8
$(Bu_4N^+)_3(Br^-)_4$	−248	−35.4
$(Bu_4N^+)_4(Br^-)_5$	−300	−33.3

Table 3. Calculated energies for dissociation pathways of $[(Et_4N^+)_4(I^-)_5]^-$.

Products of dissociation of $[(Et_4N^+)_4(I^-)_5]^-$	Calculated ΔE [kJ mol^{-1}]
$[Et_4N^+(I^-)_2]^- + [(Et_4N^+)_3(I^-)_3]^0$	+54
$[Et_4N^+(I^-)_2]^- + [(Et_4N^+)_2(I^-)_2]^0 + [Et_4N^+I^-]^0$	+100
$[Et_4N^+(I^-)_2]^- + 3[Et_4N^+I^-]^0$	+138
$2[Et_4N^+(I^-)_2]^- + [(Et_4N^+)_2I^-]^+$	+125

Conclusion

We have demonstrated the formation of stable supramolecular aggregates of tetraalkylammonium halides in the gas phase, by electrospray ionisation out of acetonitrile solution. A total of 88 aggregates with single, double and triple negative charges were recorded, the largest being $[(Bu_4N)_{39}Br_{42}]^{3-}$.

Geometrical structures for representative aggregates have been calculated, by energy minimisation using calibrated potentials for inter-ion interactions. It is concluded that the most probable structures for these supramolecular assemblies have the halide anions distributed in a matrix of cations (a fruit cake model). The calculations indicate also that the aggregates are probably quite mobile, with multiple structures on a relatively flat energy surface, separated by barriers probably less than 10 kJ mol^{-1}.

Our results provide some insight into the energies of these supramolecular assemblies, which was our main goal. Polyatomic cations can be mutually attractive, due to the van der Waals attraction exceeding the electrostatic repulsion from the dispersed positive charge. We calculate that two Bu_4N^+ ions can associate with an attractive potential energy of about 2 kJ mol^{-1}. This result is consistent with our calculations of the net attractive energies between pairs of Ph_4P^+ or $MePh_3P^+$ ions[2]and pairs of $[Ph_3PNPPh_3]^+$ ions.[30] The repulsive energies between pairs of bromide or iodide ions in these aggregates range $+2$ to $+17$ kJ mol^{-1}, while the cation$\cdots$anion attractions range up to 35 kJ mol^{-1} per pair. The accuracy of these calculated results is supported by the measured collisional dissociation of $(Et_4N^+)_4(I^-)_5$.

The calculated energies also show that there is no energy penalty in forming multiply charged ions, even when relatively small. The energy calculations are entirely consistent with the observations, the formation of large aggregates, and of multiply charged anions. It is estimated that the cohesive energies of supramolecular assemblies of ions such as these reach about 40 kJ mol^{-1} per constituent ion.

These results partly redress the serious shortage of information about the intermolecular energies of supramolecular assemblies of charged species.

Acknowledgement

This research is supported by the Australian Research Council and by the Swedish Natural Science Research Council (NFR). A travel grant to C.H. from Chalmers University of Technology is gratefully acknowledged.

[1] S. Jagner, G. Helgesson, *Adv. Inorg. Chem.* **1991**, *37*, 1 – 45.
[2] I. Dance, M. Scudder, *J. Chem. Soc. Dalton Trans.* **1996**, 3755 – 3769.
[3] I. Dance, M. Scudder, *Chem. Eur. J.* **1996**, *2*, 481 – 486.
[4] C. Hasselgren, P. A. W. Dean, M. L. Scudder, D. C. Craig, I. G. Dance, *J. Chem. Soc. Dalton Trans.* **1997**, 2019 – 2027.
[5] M. Scudder, I. Dance, *J. Chem. Soc. Dalton Trans.* **1998**, 329 – 344.
[6] M. Scudder, I. Dance, *J. Chem. Soc. Dalton Trans.* **1998**, 3155 – 3166.
[7] M. Scudder, I. Dance, *J. Chem. Soc. Dalton Trans.* **1998**, 3167 – 3176.
[8] S. Lorenzo, G. R. Lewis, I. G. Dance, *New J. Chem.* **2000**, *24*, 295 – 304.
[9] A. W. Castleman, K. H. Bowen, *J. Phys. Chem.* **1996**, *100*, 12911 – 12944.
[10] Z. Bacic, R. E. Miller, *J. Phys. Chem.* **1996**, *100*, 12945 – 12959.
[11] C. M. Whitehouse, R. N. Dreyer, M. Yamashita, J. B. Fenn, *Anal. Chem.* **1985**, *57*, 675 – 679.
[12] J. B. Fenn, M. Mann, C. K. Meng, S. F. Wong, C. M. Whitehouse, *Mass Spectrom. Rev.* **1990**, *9*, 37 – 70.
[13] R. Colton, A. D'Agostino, J. C. Traeger, *Mass Spectrom. Rev.* **1995**, *14*, 79 – 106.
[14] W. Henderson, B. K. Nicholson, L. J. McCaffrey, *Polyhedron* **1998**, *17*, 4291 – 4313.
[15] C. Hasselgren, G. Stenhagen, L. Ohrstrom, S. Jagner, *Inorg. Chim. Acta* **1999**, *292*, 266 – 271.
[16] C. E. C. A. Hop, *J. Mass Spectrom.* **1996**, *31*, 1314 – 1316.
[17] G. Wang, R. B. Cole, *J. Am. Soc. Mass. Spectrom.* **1996**, *7*, 1050 – 1058.
[18] C. E. C. A. Hop, T. B. McMahon, G. D. Willett, *Int. J. Mass Spectr. and Ion. Pro.* **1990**, *101*, 191.
[19] A. G. Marshall, C. L. Hendrickson, G. S. Jackson, *Mass Spectrom. Rev.* **1998**, 17, 1 – 35.
[20] A. J. Pertsin, A. I. Kitaigorodsky, *The atom-atom potential method. Applications to organic molecular solids, Vol. 43*, Springer, Berlin, **1987**.
[21] I. G. Dance in *The Crystal as a Supramolecular Entity* (Ed.: G. R. Desiraju), Wiley, New York, **1996**, pp. 137 – 233.
[22] B. F. Ali, I. G. Dance, M. L. Scudder, unpublished results.
[23] A. K. Rappe, W. A. Goddard, *J. Phys. Chem.* **1991**, *95*, 3358 – 3363.
[24] S. C. Harvey, *Proteins: Struc. Func. Genet.* **1989**, *5*, 78 – 92.
[25] A. Warshel, A. Papazyan, *Current Opinion in Structural Biology* **1998**, *8*, 211 – 217.
[26] D. S. Coombes, S. L. Price, D. J. Willock, M. Leslie, *J. Phys. Chem.* **1996**, *100*, 7352 – 7360.
[27] MSI, *http://www.msi.com* (**1998**) .
[28] I. G. Dance, K. J. Fisher, *J. Chem. Soc. Dalton Trans.* **1997**, 2563 – 2575.
[29] I. G. Dance, *J. Am. Chem. Soc.* **1993**, *115*, 11052 – 11053.
[30] G. R. Lewis, I. G. Dance, *J. Chem. Soc. Dalton Trans.* **2000**, 299 – 306.

Received: January 10, 2000 [F2232]

  0947-6539/00/0620-3678 $ 17.50+.50/0